

Augment Features Beyond Color for Domain Generalized Segmentation

Qiyu Sun¹, Pavlo Melnyk², Michael Felsberg², Yang Tang¹

¹ East China University of Science and Technology, ² Linköping University

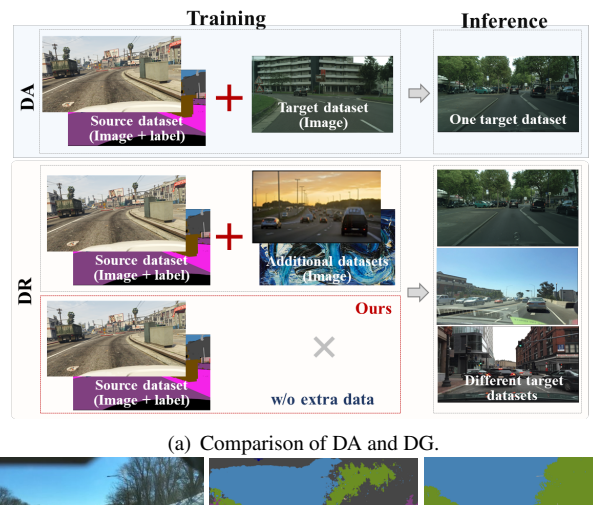
y20190063@mail.ecust.edu.cn, {pavlo.melnyk, michael.felsberg}@liu.se, yangtang@ecust.edu.cn

Abstract

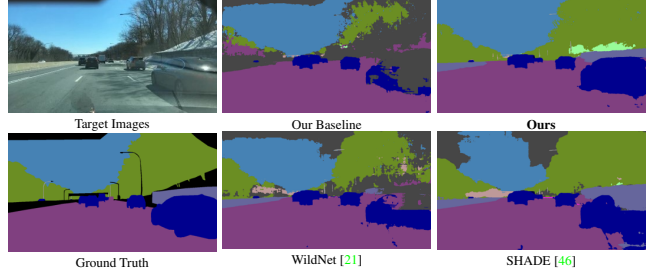
Domain generalized semantic segmentation (DGSS) is an essential but highly challenging task, in which the model is trained only on source data and any target data is not available. Previous DGSS methods can be partitioned into augmentation-based and normalization-based ones. The former either introduces extra biased data or only conducts channel-wise adjustments for data augmentation, and the latter may discard beneficial visual information, both of which lead to limited performance in DGSS. Contrarily, our method performs inter-channel transformation and meanwhile evades domain-specific biases, thus diversifying data and enhancing model generalization performance. Specifically, our method consists of two modules: random image color augmentation (RICA) and random feature distribution augmentation (RFDA). RICA converts images from RGB to the CIELAB color model and randomizes color maps in a perception-based way for image enhancement purposes. We further this augmentation by extending it beyond color to feature space using a CycleGAN-based generative network, which complements RICA and further boosts generalization capability. We conduct extensive experiments, and the generalization results from the synthetic GTAV and SYNTHIA to the real Cityscapes, BDDS, and Mapillary datasets show that our method achieves state-of-the-art performance in DGSS.

1. Introduction

The success of current deep learning-based semantic segmentation methods [1, 4, 25] comes at the price of large quantities of densely annotated images, which are extremely time-demanding and expensive to acquire [7]. Synthetic images with semantic labels generated by computer graphics can alleviate this problem by providing a relatively low-cost solution [34, 36]. However, the segmentation accuracy of models trained on synthetic datasets usually degrades dramatically when tested on real scenes due to the domain shift [10, 11]—training and test splits coming from different data distributions. In light of this, numerous tech-



(a) Comparison of DA and DG.



(b) Comparison of semantic segmentation results.

Figure 1. The problem setting (a) and qualitative results (b). DA uses the target images for training, while DG does not. Our method achieves superior generalization performance in the setting of DG but without additional data.

niques have been proposed, including domain adaptation (DA) methods [13, 27] and domain generalization (DG) approaches [6, 30, 43]. As shown in Figure 1(a), DA methods require a particular target domain for joint training with the source domain, which may be unattainable in real-world applications. Contrarily, DG approaches only need the source domain for training, rendering them more practical and promising solutions for semantic segmentation [2, 22]. This motivates us to focus our work on synthetic-to-real, domain generalized semantic segmentation (DGSS) [32].

DGSS can be broadly categorized into two main categories: normalization and whitening-based methods [6, 30–32], and domain randomization-based methods [15, 21, 33],

[43]. The former aim to obtain domain-agnostic representations by removing style information and standardizing the feature distribution, which may discard valuable information. The latter typically need additional auxiliary domain data [21, 43] to transfer the source domain images to numerous styles, as shown in Figure 1(a). However, introducing auxiliary datasets during training may lead to an undesirable inductive bias [18, 32]. To detach from auxiliary data, Zhao *et al.* [46] use AdaIN [16] to adjust the mean and standard deviation in the feature space. However, this work [46] has a limitation in the fact that it only performs channel-wise adaptive affine transformations in feature space, which ignores the interconnections between different channels and between different locations in the feature maps. As a result, a method that considers the interactions between all channels and avoids introducing domain bias is urgently needed. With this, more complex and diverse data can be generated, thereby further contributing to data diversity.

To achieve this aim, we propose two modules—random image color augmentation (RICA) and random feature distribution augmentation (RFDA). RICA conducts image augmentation on the CIELAB model [17], since it allows more comprehensible manipulation and controllable randomization on the image level [3]. While some DA methods [9, 27] also utilize CIELAB-based image augmentation to reduce the domain gap, they require the specific target domain to align each channel. In contrast, our method does not require any other dataset for distribution alignment, and instead augments data by randomizing the data distribution in each channel of the source domain solely. Experimental results demonstrate that our RICA module, while simple, can significantly enhance the performance of DGSS.

While RICA introduces some variations in the color map, it only conducts color-based augmentation and thus has limitations in accounting for other important factors that contribute to image diversity, like texture. To overcome this limitation, RFDA is proposed to stylize feature maps during forward propagation, allowing for joint augmentation of all channels and considering the interactions between channels. RFDA leverages and modifies the architecture of the CycleGAN-based model [47] to obtain a feature generator, named Feature GAN, in this work. Incorporating Feature GAN to generate stylized features instead of AdaIN [16] enhances the model’s augmentation power by capturing the correlations between different channels and locations within feature maps. It is worth noting that though previous works have employed CycleGAN for numerous tasks, to the best of our knowledge, our proposed RFDA is the first to utilize the CycleGAN-based model for data stylization in *feature* space for DS GG. The training data for Feature GAN are the images augmented by RICA, and thus we avoid introducing auxiliary datasets and undesirable biases.

In summary, the proposed RICA and RFDA operate in a complementary manner to conduct data augmentation in both image and feature space, enabling segmentation networks to generalize to unseen target data, and achieve state-of-the-art performance, as shown in Figure 1(b). The contributions of our work are summarized as follows:

- 1) We propose a perception-based effective image color randomization mechanism named RICA, for DGSS. It eliminates the need for an auxiliary dataset during training and relies only on the source domain.
- 2) We propose the innovative RFDA with a CycleGAN-based architecture to perform cross-channel feature synthesis, enabling the model to generate complementary features to the color-based augmentation.
- 3) Extensive experiments conducted on benchmark datasets and multiple domain generalization tasks show that our proposed RICA and RFDA strategies operating in combination achieve state-of-the-art generalization results.

2. Related Work

In this section, we introduce related literature on synthetic-to-real semantic segmentation, including domain adaptation (DA) and domain generalization (DG).

DA for semantic segmentation. To bridge the gap between source and target domain, existing works prioritize domain adaption (DA) techniques, which cater to a particular target domain by jointly learning from labeled source-domain data and often-unlabeled target data. Unsupervised DA (UDA) is the most attractive among different DA variants in semantic segmentation because the target domain is unlabeled in this setting, and hence, is less demanding. The mainstream UDA semantic segmentation methods can be divided into three categories: input-based (image translation) [13, 19, 27], feature-based (feature alignment) [14, 26, 29], and output-based (segmentation alignment) [24, 38, 40]. Even though DA increases the performance of the model on target domain data to a large extent, it requires concurrent access to both source and target data, which is impractical and cannot be generalized to new target domains not seen during training.

DG for semantic segmentation. Recently, simulation-to-real semantic segmentation has begun to bring itself into purview due to its prospective real-world application prospect. In this line of work, the segmentation network is trained on synthetic domains and then tested on unseen real target domains. Unlike DA approaches exploiting target domain data during training, DG methods utilize only the source domain and aim to generalize to multiple unseen target domains. Existing DG methods can be divided into two groups [32]: 1) normalization and whitening and 2) domain randomization. Additionally, some other works [18, 44] employ meta-learning-based methods for DGSS.

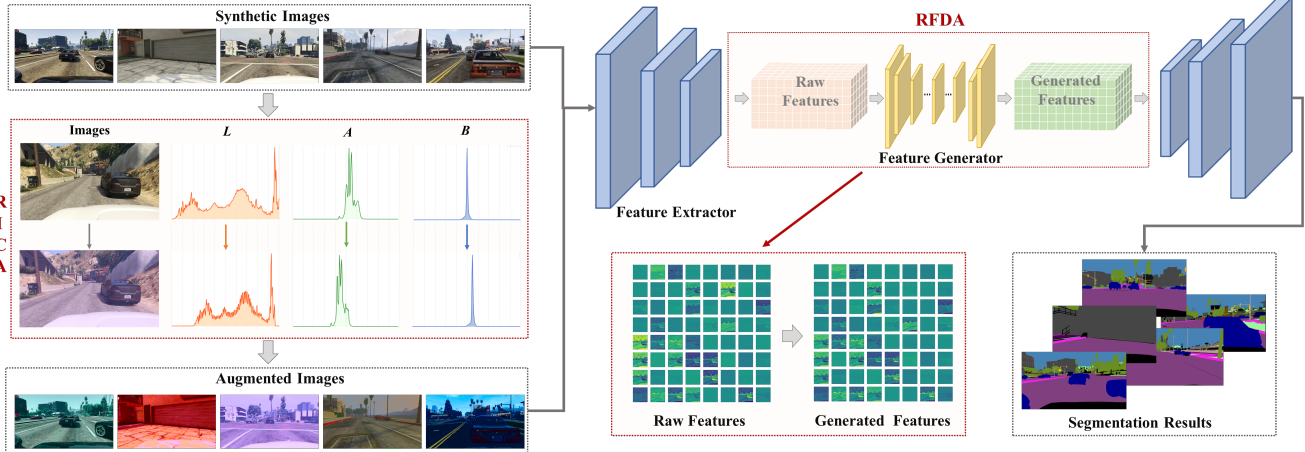


Figure 2. The training framework of our method: To generate new images with input-level data augmentation, we begin by inputting raw synthetic images into RICA. Subsequently, both the original and augmented images are input into the segmentation model. The extracted features are further enhanced through our pre-trained Feature Generator (the generator of Feature GAN) in the feature space. We utilize RICA exclusively during the training process, while we retain RDFA for inference purposes.

Normalization and whitening methods utilize such techniques as instance normalization (IN) [39] or instance whitening (IW) [23] to standardize the feature distribution of different samples. Pan *et al.* [30] propose a network architecture that is comprised of instance normalization (IN) and batch normalization (BN) to learn style-invariant features and preserve content information. Choi *et al.* [6] suggest it is the style of images that causes domain shift, and thus disentangle features into style and content to selectively remove domain-specific style information. Xu *et al.* [41] employ feature sensitivity as the feature prior to enhancing the model’s generalization capability. On top of extracting domain-agnostic features, Peng *et al.* [32] align category-level centers of different domains to obtain intra-category compactness.

Domain randomization methods heuristically explore the characteristics of potentially unpredictable target domains and try to generate multifarious styles of images for training from the source domain. Several works conduct data augmentation in image space [15,33,43] and some explore data manipulation in feature space [20, 21, 37, 46]. Some studies [15, 21, 43] employ ImageNet [8] as an auxiliary dataset for domain randomization. For instance, Yue *et al.* [43] employ CycleGAN to randomize the source domain, Huang *et al.* [15] manipulate images in the frequency domain for easier handling and preservation of semantic structures, while Lee *et al.* [21] diversify the source image styles by aligning the characteristics of source domain features with those of images in ImageNet. Other datasets are also utilized for domain randomization in some works [20,33]. Peng *et al.* [33] and Tjio *et al.* [37] merge the styles of unreal paintings to generate diverse textures for source images, while Kim *et al.* [20] inject web-crawled style representations into the source domain. Moreover, Zhao *et al.* [46] generate diverse

training samples by selecting basis styles from the source distribution, without relying on additional datasets as done by previous works.

Our method belongs to the domain randomization category and it stands out by not requiring additional datasets. Unlike [46] which performs feature augmentation in separate channels by adjusting only the mean and standard deviation with AdaIN [16], our method leverages a CycleGAN-based module to generate more diverse and informative features.

3. Method

In this section, we describe the two data-augmentation modules we propose to solve the DGSS problem—random image color augmentation (RICA) and random feature distribution augmentation (RFDA). By their use, we jointly enhance the diversity of data in both image and feature space. In particular, RICA aims to change the statistical distribution of the given source domain in image space. At the same time, RFDA improves the generalizability of the model by stylizing the features. Our main framework is shown in Figure 2. First, the source images are fed into RICA for color augmentation. Then, the raw and augmented images are fed into our designed semantic segmentation model for training. Unlike a traditional segmentation model pipeline, we integrate a feature generator into the model to perform inter-channel feature augmentation.

3.1. Random Image Color Augmentation (RICA)

The vast majority of previous works [15, 21, 33, 43] rely on additional auxiliary domain data to transfer the source domain images to numerous styles. On the contrary, our proposed RICA strategy aims to augment source-domain images using no auxiliary data. Our main intuition is that



Figure 3. Color augmentation with RICA: Input images (left-most column) and RICA output (the remaining columns). By adjusting the values in *LAB* channels, RICA produces a range of images that retain their original semantic contents.

RICA can deal with unseen target domains because it generates different kinds of statistical distributions, which prevent the segmentation model from over-fitting the characteristics of the given source data. Consequently, the segmentation model can be more robust with respect to various data distributions across arbitrary unseen domains.

To conduct meaningful image augmentation, our idea is to use a color representation that is more intuitive for humans than the original RGB color model. Therefore, we convert the images into the CIELAB model [17] since it is designed to imitate human vision. The CIELAB color model contains three channels to express color: *L* for perceptual lightness, *A* and *B* for four colors of human vision, depicting the shift from green to red and blue to yellow, respectively.

We use this human-perception-friendly color representation, because it allows us to augment the source data by randomly modifying the value of the three CIELAB channels, while **preserving the semantic content** of the original images. We hypothesize that this augmentation can endow the training set with the different characteristics of various other datasets, improving the domain generalizability of the model. To perform this augmentation, we first randomize the channel-wise mean and standard deviation in the three channels (RICA-Step1):

$$M^c = \sigma(M^c) \cdot \left(\frac{R^c - \mu(R^c)}{\sigma(R^c)} \right) + \mu(M^c), \quad (1)$$

where R^c is the raw color channels $c \in \{L, A, B\}$, M^c is the corresponding color channels after the random augmentation of RICA-Step1. $\mu(*)$ and $\sigma(*)$ represents the channel-wise mean and standard deviation. Noteworthy, the value range of M^c is clipped to $[0, 255]$, which works like a two-sided ReLU.

Then, we utilize the following linear mapping (RICA-

Step2):

$$\begin{aligned} N^c &= \frac{N_{\max}^c - N_{\min}^c}{M_{\max}^c - M_{\min}^c} \cdot (M^c - M_{\min}^c) + N_{\min}^c \\ &= \frac{M^c - M_{\min}^c}{M_{\max}^c - M_{\min}^c} \cdot (N_{\max}^c - N_{\min}^c) + N_{\min}^c, \end{aligned} \quad (2)$$

where M_{\max}^c and M_{\min}^c are the maximum and minimum values of the channel M^c , N_{\max}^c and N_{\min}^c are the maximum and minimum values of the modified interval after RICA-Step2.

Let $S^c = N_{\max}^c - N_{\min}^c$ be the range of the modified interval and $T^c = N_{\min}^c$ be the starting point of the interval, then we obtain

$$N^c = \frac{M^c - M_{\min}^c}{M_{\max}^c - M_{\min}^c} \cdot S^c + T^c. \quad (3)$$

We randomly select the value of $\mu(M^c)$, $\sigma(M^c)$, S^c and T^c for image color expansion in each channel $c \in \{L, A, B\}$.

To sum up, we conduct diverse randomization in CIELAB color representation and then convert the images back to the RGB model for further training. In RICA, we enlarge the range of each of the *LAB* channels, which creates new, richer data distributions to train the segmentation model. As shown in Figure 2, RICA changes the characteristics of each channel and thus generates new images with different color styles. More examples generated by RICA are shown in Figure 3: as we can see, the image semantics are preserved, while the color is expanded.

3.2. Random Feature Distribution Augmentation (RFDA)

We explore whether we can generate multifarious distributions of features using GANs to diversify the characteristics of the features extracted from the source domain and thereby adapt to various other domains. Complementary to RICA, we design RFDA with Feature GAN being its main component.

The architecture of Feature GAN is inspired by CycleGAN [47]. In particular, we remove the first and last CNN layers of the generator in CycleGAN to generate feature maps instead of images and keep the original discriminator. The training pipeline of RFDA is shown in Figure 4, and the specific training steps are discussed in Section 3.3.

To train Feature GAN, we need to collect real samples. We refer to the part of the segmentation model from the input through the chosen layer as the *real*¹ feature extractor F . The loss function of Feature GAN is also similar to CycleGAN, except that, instead of using L1 loss for cycle consistency loss, we use Kullback–Leibler (KL) divergence to calculate the distance between the real features extracted by F and the features generated by the generator. This is

¹Real as opposed to fake in terms of the GAN training.

because L1 loss is commonly used for calculating the differences between images, while KL divergence is more suitable for measuring the distance between feature maps [45]. Hence, the cycle consistency loss for Feature GAN becomes

$$\begin{aligned} \mathcal{L}_{\text{cyc}}(G_A, G_B) = & \mathbb{E}_{f_A \sim p_{\text{data}}(f_A)} [\text{KL}(G_B(G_A(f_A)) || f_A)] \\ & + \mathbb{E}_{f_B \sim p_{\text{data}}(f_B)} [\text{KL}(G_A(G_B(f_B)) || f_B)], \end{aligned} \quad (4)$$

where G_A, G_B are the two generators, f_A, f_B are the real features extracted by F from two domains.

The impressive generation capability of GAN enables RFDA to effectively capture the interconnections across different feature channels and leverage the spatial information contained within feature maps.

3.3. Training Steps

The training of our method can be divided into three steps. First, we train the baseline segmentation model with images augmented by RICA to obtain the real feature extractor F , as shown in Figure 4(a). Second, we train Feature GAN using F obtained in Step 1, as shown in Figure 4(b). Finally, we plug the generator G_A of Feature GAN, further referred to simply as G , into the model, as shown in Figure 4(c), and perform the model training anew.

Step 1: Train the real feature extractor F . We train the baseline semantic segmentation model with both raw and RICA-augmented images to obtain the feature extractor F . Note that the generator G can be inserted in the segmentation model after any chosen layer. If we choose it to be the first convolutional layer of the model, our F will consist of only one layer, as illustrated in Figure 4.

Step 2: Train the Feature GAN. We fix the parameters of F trained in Step 1 and utilize F to generate real samples. Since Feature GAN aims to generate as many different styles of features as possible while maintaining their underlying semantic contents, the training samples (*i.e.*, extracted features) should come from the same image but in different styles. Thus, we augment the source domain images using RICA, and then feed them into F to obtain real samples to train Feature GAN.

Step 3: Integrate Feature GAN into the segmentation model. After Feature GAN is trained, we fix the parameters of the generator and integrate it into the segmentation model, right after F , as shown in Figure 4(c). Then, we train the new segmentation model with both raw images and the images augmented by RICA. Just like in Step 1: The output of F is fed into Feature GAN which subsequently generates new, modified features, which are propagated into the following layers of the segmentation model.

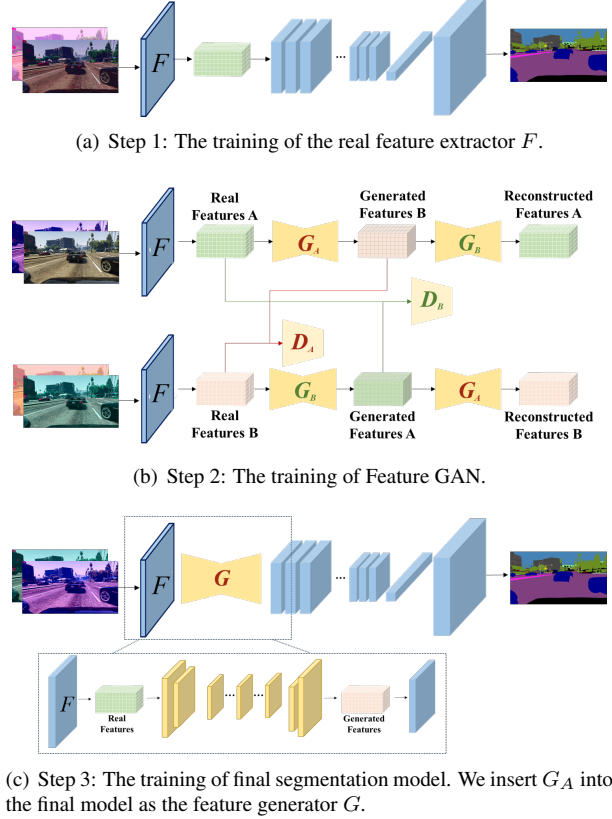


Figure 4. Training steps of our method, described in Section 3.3.

4. Experiments

4.1. Experimental Setup

4.1.1 Datasets

In our experiments, we utilize two synthetic datasets as source domains (GTAV [34] and SYNTHIA [36]) and three real datasets as target domains (Cityscapes [7], Berkeley Deep Drive Segmentation (BDDS) [42], and Mapillary [28]). In the following, we introduce each dataset in detail.

Synthetic datasets. GTAV is collected from the game Grand Theft Auto V and contains 24,966 images. It is split into train, validation, and test sets, which consist of 12,403, 6,382, and 6,181 images, respectively. The subset of SYNTHIA, SYNTHIA-RAND-CITYSCAPES, is also used in our experiments, and contains 9,400 images and is split into 6,580 and 2,820 images for training and validation, following the convention in [6, 21]. All of the synthetic datasets have pixel-wise semantic labels for training.

Real datasets. Cityscapes contains 5,000 images, 2,975, 500, and 1,525 for training, validation, and test. BDDS contains 10,000 images, and its training, validation, and test sets contain 7,000, 1,000, and 2,000 images, respectively. Mapillary has a training set with 18,000 images and a validation set with 2,000 images.

Table 1. Comparison of mIoU (%) under DGSS setting using the backbone of ResNet-50 and ResNet-101. The source domain is GTAV (G), SYNTHIA (S), respectively, and the unseen target domains are Cityscapes (C), BDDS (B), and Mapillary (M). The best and second best results are highlighted in **bold** and underline. “Auxiliary data” refers to any additional data used besides G and S. “Baseline” represents the original basic model reported in the corresponding compared works. “/” means the result is not reported in the original paper.

Backbone	Method	Auxiliary data	Train on GTAV (G)				Train on SYNTHIA (S)			
			→ C	→ B	→ M	Average	→ C	→ B	→ M	Average
ResNet-50	Baseline		22.20	/	/	/	/	/	/	/
	IBN-Net [30]	×	29.60	/	/	/	/	/	/	/
	Baseline	✓	32.45	26.73	25.66	28.28	28.36	25.16	27.24	26.92
	DRPC [43]		37.42	32.14	34.12	34.56	<u>35.65</u>	31.53	32.74	33.31
	Baseline		28.95	25.14	28.18	27.42	/	/	/	/
	RobustNet [6]	×	36.58	35.20	40.33	37.37	/	/	/	/
	Baseline	✓	31.70	/	/	/	/	/	/	/
	GLTR [33]		38.60	/	/	/	/	/	/	/
	Baseline		29.32	25.71	28.33	27.79	23.18	24.50	21.79	23.16
	SAN-SAW [32]	×	39.75	37.34	41.86	39.65	<u>38.92</u>	<u>35.24</u>	<u>34.52</u>	<u>36.23</u>
	Baseline	✓	35.16	29.71	31.29	32.05	/	/	/	/
	WildNet [21]		44.62	38.42	46.09	43.04	/	/	/	/
ResNet-101	Baseline		28.95	25.14	28.18	27.42	/	/	/	/
	SHADE [46]	×	44.65	<u>39.28</u>	43.34	42.42	/	/	/	/
	Baseline		33.29	33.88	36.30	34.49	36.30	26.14	30.47	30.97
	Ours	×	47.82	41.86	46.23	45.30	44.50	35.41	39.13	39.68
	Baseline	✓	33.56	27.76	28.33	29.88	29.67	25.64	28.73	28.01
	DRPC [43]		42.53	38.72	38.05	39.77	37.58	34.34	34.12	35.35
	Baseline	✓	33.40	27.30	27.90	29.53	/	/	/	/
	FSDR [15]		44.80	41.20	43.40	43.13	40.80	37.40	<u>39.60</u>	<u>39.27</u>
	Baseline	✓	34.00	28.10	28.60	30.23	30.20	25.90	29.50	28.53
	GLTR [33]		43.70	39.60	39.10	40.80	39.70	35.30	36.40	37.13
	Baseline		30.64	27.82	28.65	29.04	23.85	25.01	21.84	23.57
	SAN-SAW [32]	×	45.33	41.18	40.77	42.43	<u>40.87</u>	35.98	37.26	38.04
	Baseline	✓	35.73	34.06	33.42	34.40	/	/	/	/
	WildNet [21]		45.79	41.73	47.08	44.87	/	/	/	/
	Baseline		32.97	30.77	30.68	31.47	/	/	/	/
	SHADE [46]	×	<u>46.66</u>	<u>43.66</u>	45.50	<u>45.27</u>	/	/	/	/
	Baseline	×	34.48	35.78	38.26	36.17	36.39	28.61	32.84	32.61
	Ours	×	48.03	45.19	<u>46.26</u>	46.49	44.99	<u>36.25</u>	41.60	40.95

4.1.2 Implementation Details

We use DeeplabV3+ [5]² as the semantic segmentation network in all the experiments. To conduct a fair comparison with existing methods [6, 15, 21, 30, 32, 33, 43, 46], we adopt standard ResNet-50 and ResNet-101 [12] as the feature extraction backbones. Our experiments are run on a single NVIDIA A40 GPU. The networks are trained with SGD as an optimizer [35] with a weight decay of 10^{-4} and momentum of 0.9. The initial learning rates of the backbone and classifier are $2.5 \cdot 10^{-3}$ and $2.5 \cdot 10^{-2}$, respectively, and they decrease with a power of 0.9 using the polynomial policy. The models are trained for 60k iterations when trained on a single synthetic dataset, while trained for 120k iterations when trained on both of the two synthetic datasets. The training batch size is set to 8 in the experiments. We also apply several basic augmentations in experiments, including random scale, random rotation, random crop, color jitter, and random horizontal flip, following the other methods [6, 21]. Determined empirically, we randomly select $\mu(M^c)$ from 0 to 255 for each channel, with $\sigma(M^c)$ from 0

to 100, S^c from 30 to 255 for illumination channel L , and $\sigma(M^c)$ from 0 to 15, S^c from 30 to 220 for color channels A and B in RICA.

For the training of Feature GAN, we use all the images in the source domain and perform RICA to extract real features by means of F , and train Feature GAN for 10 epochs. The number of input channels for Feature GAN is equivalent to the number of output channels extracted by F .

In our experiments, we choose the 19 categories that overlap with Cityscapes in both training and testing when utilizing GTAV as the source domain, while 16 categories are used when training on SYNTHIA only. We evaluate the performance of our segmentation model using the mean intersection over union (mIoU) of the chosen categories. Unless otherwise stated, we insert Feature GAN after the first convolutional layer to obtain the best results. More implementation details are provided in the supplementary material.

4.2 Results

Quantitative comparisons are made between our method and the existing DGSS methods: IBN-Net [30], DRPC [43],

²<https://github.com/VainF/DeepLabV3Plus-Pytorch>

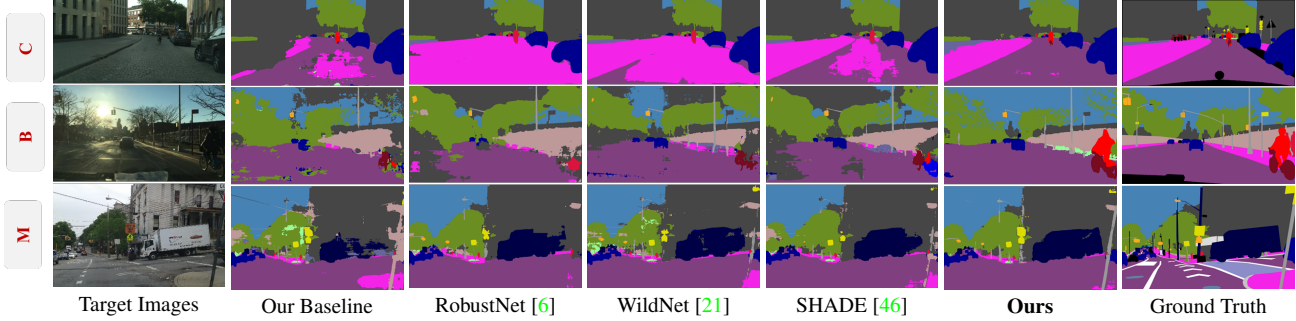


Figure 5. Visual comparison of different models trained with ResNet-50 backbone (G→ C, B, M). For a fair comparison, we utilize the models provided by the authors [6, 21, 46] for visualization. Although three state-of-the-art methods (RobustNet [6], WildNet [21], and SHADE [46]) have improved the average mIoU on three real datasets to 37.37%, 43.04%, and 42.42%, their performance is still limited. Our method achieves superior generalization performance with an average mIoU of 45.30% by jointly synthesizing the color and feature maps, significantly outperforming the baseline. More qualitative results on the three datasets are available in the supplementary material.

Table 2. Comparison of mIoU (%) under the DGSS setting using the backbone of ResNet-50. The models are trained with multiple synthetic datasets (G + S → C, B, M).

Methods	G + S → C	G + S → B	G + S → M	Average
Baseline	35.46	25.09	31.94	30.83
RobustNet [6]	37.69	34.09	38.49	36.76
Baseline	35.46	25.09	31.94	30.83
Kim <i>et al.</i> [18]	44.51	38.07	42.70	41.76
Baseline	35.46	25.09	31.94	30.83
SHADE [46]	47.43	40.30	47.60	45.11
Baseline	37.99	34.29	37.37	36.55
Ours	47.36	43.45	48.13	46.31

FSDR [15], RobustNet [6], GLTR [33], SAN-SAW [32], WildNet [21], and SHADE [46]. We use GTAV and SYNTHIA separately as the source domain to train our model and then test it on the three unseen real-world datasets—Cityscapes, BDDS, and Mapillary. Table 1 shows a comprehensive quantitative comparison of the semantic segmentation generalization performance of several models with ResNet-50 and ResNet-101 backbones. Our method achieves remarkably high generalization performance over multiple domains, while surpassing all the other methods using the ResNet-50 backbone, and being the best in all but two (G→M and S→B) comparisons for the ResNet-101 backbone. To conceptualize the segmentation results, we present some qualitative results on each target domain in Figure 5. As we can see from the figure, our method can distinguish not only two easily-confused categories, *sidewalk* and *road* (row 1), but also various other objects, *e.g.*, *rider*, *truck*, and *traffic sign*. Furthermore, our method performs reliably in scenarios containing specular reflection (Figure 1(b)) and low illumination (row 2).

We also conduct experiments of multi-domain generalization, which means training on both GTAV and SYNTHIA and then testing on unseen real domains. Both the results of our method and the results available in related work are shown in Table 2. Once again, our method demonstrates superior performance compared to the existing approaches.

Table 3. Ablation studies on RICA and RFDA (G→ C, B, M). “Baseline” denotes the original DeeplabV3+ using ResNet-50 backbone. The results are reported with mIoU (%).

Methods	RICA	RFDA	G→ C	G→ B	G→ M	Average
Baseline	✗	✗	33.29	33.88	36.30	34.49
Baseline + RICA	✓	✗	45.19	41.50	43.95	43.55
Baseline + RFDA	✗	✓	36.88	41.00	41.72	39.87
All (Ours)	✓	✓	47.82	41.86	46.23	45.30

4.3. Ablation Studies

We conduct ablation experiments using the ResNet-50 backbone, generalizing from GTAV to Cityscapes, BDDS, and Mapillary. First, we evaluate the effectiveness of our proposed RICA and RFDA modules to see how they influence the model performance. The results are shown in Table 3, where Baseline represents the original DeeplabV3+ semantic segmentation model.

The baseline model overfits the source domain and shows poor capability on real datasets. On the other hand, when only RICA is applied, the model achieves a remarkably higher average mIoU of 43.55% on four datasets with a +9.06% improvement. When only RFDA is utilized, the model achieves an average mIoU of 39.87% with a +5.38% improvement. The combination of the two modules further boosts the model performance, attaining an average mIoU of 45.30% with a +10.81% improvement. This confirms that RICA and RFDA work in a complementary manner. In the following, we conduct more detailed ablation experiments for our RICA and RFDA modules.

RICA in different channels. Table 4 reports the influence of each *LAB* channel on model generalization, along with the two randomization steps of RICA. Clearly, randomization in all channels leads to improvements, and both steps contribute to this improvement. Additionally, we perform the identical randomization used in RICA in the RGB color model, and explore the influence of hyperparameters of $\mu(M^c)$, $\sigma(M^c)$, and S^c . All the corresponding results are provided in the supplementary material.

RFDA in different layers. We also explore the impact

Table 4. Ablation studies on RICA in ResNet-50 backbone ($G \rightarrow C, B, M$). L, A , and B denote conducting data augmentation only in a single channel. “RICA-Step1” and “RICA-Step2” denote the two randomization steps introduced in Section 3.1. The reported results are mIoU (%).

Method	Channel			$G \rightarrow C$	$G \rightarrow B$	$G \rightarrow M$	Average
	L	A	B				
Baseline	x	x	x	33.29	33.88	36.30	34.49
Baseline + L	✓	x	x	34.10	37.08	38.94	36.71
Baseline + A	x	✓	x	44.74	39.95	43.95	42.88
Baseline + B	x	x	✓	44.89	41.13	43.45	43.15
Baseline + RICA-Step1	✓	✓	✓	44.13	40.41	43.62	42.72
Baseline + RICA-Step2	✓	✓	✓	45.40	38.29	42.42	42.04
Baseline + RICA	✓	✓	✓	45.19	41.50	43.95	43.55

Table 5. Ablation studies on the position of feature generator G in ResNet-50 backbone ($G \rightarrow C, B, M$).

Position of G	$G \rightarrow C$	$G \rightarrow B$	$G \rightarrow M$	Average
w/o G	45.19	41.50	43.95	43.55
G After Conv1	47.82	41.86	46.23	45.30
G After Block Group1	46.34	41.67	43.60	43.87
G After Block Group2	46.47	39.60	44.40	43.49

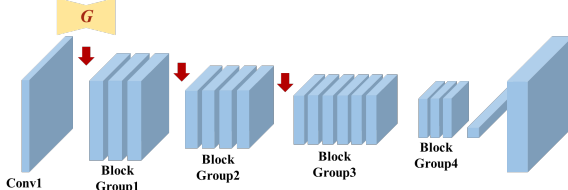


Figure 6. The illustration of the position of feature generator G .

of the position of the feature generator G in the segmentation model, as illustrated in Figure 6. Namely, we use the features produced by the first convolutional layer, and then the first and second block groups for the respective Feature GAN training. The results are shown in Table 5. As we can see, placing RFDA deeper after Block Group 2 performs a little worse than the baseline. It is explicable since deeper layers extract higher-level semantic information, and thus altering the high-level features can remove important details and edit semantic contents. On the contrary, augmenting the first layer features preserves the valuable context information and vary style information, which is beneficial for the segmentation task, as indicated by the higher performance of RICA when placed after Conv1 (see Table 5).

4.4. Further Analysis

RICA. To gain a better understanding of why RICA is so effective, we randomly select 100 images from each dataset and illustrate the distribution in channels A , as shown in Figure 7. From Figure 7(a), the overlap of the value range between synthetic datasets (G and S in red) and real datasets (C, B, and M in green) is quite small. We argue that this difference in data distributions, to some extent leads to the domain shift in semantic segmentation. Since the value is concentrated in a small range, we locally zoom in on the range

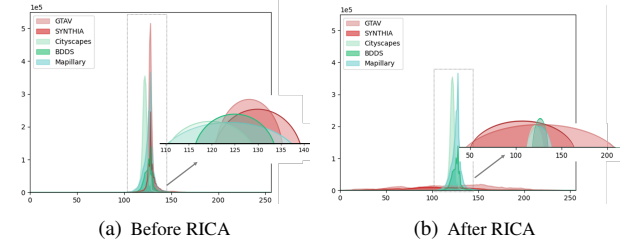


Figure 7. Data distribution of different datasets in channel A . The zoomed-in regions are to display the overlap of the value ranges, and the relative height is arbitrary. After RICA, the value range of the synthetic data covers the whole distribution of the real data.

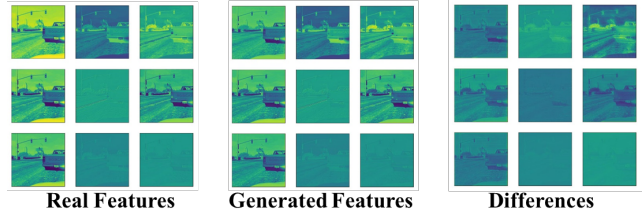


Figure 8. Augmentation with RFDA. Left: input (real) features. Middle: features produced by Feature GAN. Right: the differences between the two.

and visualize the distribution of the range in a more intuitive way. As shown in Figure 7(b), our method expands the channel value range of synthetic datasets to cover the whole distribution of real datasets. This effectively augments the source data, enhancing the generalization capability of the segmentation model.

RFDA. We visualize the features extracted by F (real features), the features generated by G (generated features), and their difference in Figure 8. In Figure 8, G is inserted after the first convolutional layer, and we choose 9 channels for better illustration. As is shown, our Feature GAN indeed stylizes the features while preserving their semantic contents.

5. Conclusion

In this paper, we present a novel method for synthetic-to-real DGSS based on joint image and feature augmentation, which is carried out by our proposed RICA and RFDA modules. Quantitative and qualitative results clearly indicate that our method exhibits notable generalization capabilities on different unseen target domains while using different backbones and source domains, achieving state-of-the-art results. The conducted ablation studies verify that RICA and RFDA best work in a complementary manner, opening the door to an entirely new scope of possible future developments. Since RICA relies on appropriate hyper-parameter selection, further investigation is required to elevate its effectiveness, which may promote the performance of RFDA as well. One promising direction is to alter the manual hyper-parameter selection with a learning-based module.

References

- [1] Vijay Badrinarayanan, Alex Kendall, and Roberto Cipolla. Segnet: A deep convolutional encoder-decoder architecture for image segmentation. *IEEE transactions on pattern analysis and machine intelligence*, 39(12):2481–2495, 2017. 1
- [2] Yogesh Balaji, Swami Sankaranarayanan, and Rama Chellappa. Metareg: Towards domain generalization using meta-regularization. *Advances in Neural Information Processing Systems*, 31:998–1008, 2018. 1
- [3] Amanda Berg, Jorgen Ahlberg, and Michael Felsberg. Generating visible spectrum images from thermal infrared. In *Proceedings of the IEEE Conference on Computer Vision and Pattern Recognition Workshops*, pages 1143–1152, 2018. 2
- [4] Liang-Chieh Chen, George Papandreou, Iasonas Kokkinos, Kevin Murphy, and Alan L Yuille. Deeplab: Semantic image segmentation with deep convolutional nets, atrous convolution, and fully connected crfs. *IEEE transactions on pattern analysis and machine intelligence*, 40(4):834–848, 2017. 1
- [5] Liang-Chieh Chen, Yukun Zhu, George Papandreou, Florian Schroff, and Hartwig Adam. Encoder-decoder with atrous separable convolution for semantic image segmentation. In *Proceedings of the European conference on computer vision (ECCV)*, pages 801–818, 2018. 6
- [6] Sungha Choi, Sanghun Jung, Huiwon Yun, Joanne T Kim, Seungryong Kim, and Jaegul Choo. Robustnet: Improving domain generalization in urban-scene segmentation via instance selective whitening. In *Proceedings of the IEEE/CVF Conference on Computer Vision and Pattern Recognition*, pages 11580–11590, 2021. 1, 3, 5, 6, 7
- [7] Marius Cordts, Mohamed Omran, Sebastian Ramos, Timo Rehfeld, Markus Enzweiler, Rodrigo Benenson, Uwe Franke, Stefan Roth, and Bernt Schiele. The cityscapes dataset for semantic urban scene understanding. In *Proceedings of the IEEE conference on computer vision and pattern recognition*, pages 3213–3223, 2016. 1, 5
- [8] Jia Deng, Wei Dong, Richard Socher, Li-Jia Li, Kai Li, and Li Fei-Fei. Imagenet: A large-scale hierarchical image database. In *2009 IEEE conference on computer vision and pattern recognition*, pages 248–255. Ieee, 2009. 3
- [9] Lidia Fantauzzo, Eros Fani, Debora Caldarola, Antonio Tavera, Fabio Cermelli, Marco Ciccone, and Barbara Caputo. Feddrive: generalizing federated learning to semantic segmentation in autonomous driving. In *2022 IEEE/RSJ International Conference on Intelligent Robots and Systems (IROS)*, pages 11504–11511. IEEE, 2022. 2
- [10] Yaroslav Ganin and Victor Lempitsky. Unsupervised domain adaptation by backpropagation. In *International conference on machine learning*, pages 1180–1189. PMLR, 2015. 1
- [11] Yaroslav Ganin, Evgeniya Ustinova, Hana Ajakan, Pascal Germain, Hugo Larochelle, François Laviolette, Mario Marchand, and Victor Lempitsky. Domain-adversarial training of neural networks. *The journal of machine learning research*, 17(1):2096–2030, 2016. 1
- [12] Kaiming He, Xiangyu Zhang, Shaoqing Ren, and Jian Sun. Deep residual learning for image recognition. In *Proceedings of the IEEE conference on computer vision and pattern recognition*, pages 770–778, 2016. 6
- [13] Judy Hoffman, Eric Tzeng, Taesung Park, Jun-Yan Zhu, Phillip Isola, Kate Saenko, Alexei Efros, and Trevor Darrell. Cycada: Cycle-consistent adversarial domain adaptation. In *International conference on machine learning*, pages 1989–1998. Pmlr, 2018. 1, 2
- [14] Judy Hoffman, Dequan Wang, Fisher Yu, and Trevor Darrell. Fcns in the wild: Pixel-level adversarial and constraint-based adaptation. *arXiv preprint arXiv:1612.02649*, 2016. 2
- [15] Jiaxing Huang, Dayan Guan, Aoran Xiao, and Shijian Lu. Fsdr: Frequency space domain randomization for domain generalization. In *Proceedings of the IEEE/CVF Conference on Computer Vision and Pattern Recognition*, pages 6891–6902, 2021. 1, 3, 6, 7
- [16] Xun Huang and Serge Belongie. Arbitrary style transfer in real-time with adaptive instance normalization. In *Proceedings of the IEEE international conference on computer vision*, pages 1501–1510, 2017. 2, 3
- [17] Noor A Ibraheem, Mokhtar M Hasan, Rafiqul Z Khan, and Pramod K Mishra. Understanding color models: a review. *ARPN Journal of science and technology*, 2(3):265–275, 2012. 2, 4
- [18] Jin Kim, Jiyoung Lee, Jungin Park, Dongbo Min, and Kwanghoon Sohn. Pin the memory: Learning to generalize semantic segmentation. In *Proceedings of the IEEE/CVF Conference on Computer Vision and Pattern Recognition*, pages 4350–4360, 2022. 2, 7
- [19] Myeongjin Kim and Hyeran Byun. Learning texture invariant representation for domain adaptation of semantic segmentation. In *Proceedings of the IEEE/CVF conference on computer vision and pattern recognition*, pages 12975–12984, 2020. 2
- [20] Namyp Kim, Taeyoung Son, Cuiling Lan, Wenjun Zeng, and Suha Kwak. Wedge: web-image assisted domain generalization for semantic segmentation. *arXiv preprint arXiv:2109.14196*, 2021. 3
- [21] Suhyeon Lee, Hongje Seong, Seongwon Lee, and Euntai Kim. Wildnet: Learning domain generalized semantic segmentation from the wild. In *Proceedings of the IEEE/CVF Conference on Computer Vision and Pattern Recognition*, pages 9936–9946, 2022. 1, 2, 3, 5, 6, 7
- [22] Da Li, Yongxin Yang, Yi-Zhe Song, and Timothy M Hospedales. Learning to generalize: Meta-learning for domain generalization. In *Thirty-Second AAAI Conference on Artificial Intelligence*, 2018. 1
- [23] Yijun Li, Chen Fang, Jimei Yang, Zhaowen Wang, Xin Lu, and Ming-Hsuan Yang. Universal style transfer via feature transforms. *Advances in neural information processing systems*, 30, 2017. 3
- [24] Yuang Liu, Wei Zhang, and Jun Wang. Source-free domain adaptation for semantic segmentation. In *Proceedings of the IEEE/CVF Conference on Computer Vision and Pattern Recognition*, pages 1215–1224, 2021. 2
- [25] Jonathan Long, Evan Shelhamer, and Trevor Darrell. Fully convolutional networks for semantic segmentation. In *Proceedings of the IEEE conference on computer vision and pattern recognition*, pages 3431–3440, 2015. 1

[26] Yawei Luo, Ping Liu, Tao Guan, Junqing Yu, and Yi Yang. Significance-aware information bottleneck for domain adaptive semantic segmentation. In *Proceedings of the IEEE/CVF International Conference on Computer Vision*, pages 6778–6787, 2019. [2](#)

[27] Haoyu Ma, Xiangru Lin, Zifeng Wu, and Yizhou Yu. Coarse-to-fine domain adaptive semantic segmentation with photometric alignment and category-center regularization. In *Proceedings of the IEEE/CVF Conference on Computer Vision and Pattern Recognition*, pages 4051–4060, 2021. [1, 2](#)

[28] Gerhard Neuhold, Tobias Ollmann, Samuel Rota Bulo, and Peter Kontschieder. The mapillary vistas dataset for semantic understanding of street scenes. In *Proceedings of the IEEE international conference on computer vision*, pages 4990–4999, 2017. [5](#)

[29] Fei Pan, Inkyu Shin, Francois Rameau, Seokju Lee, and In So Kweon. Unsupervised intra-domain adaptation for semantic segmentation through self-supervision. In *Proceedings of the IEEE/CVF Conference on Computer Vision and Pattern Recognition*, pages 3764–3773, 2020. [2](#)

[30] Xingang Pan, Ping Luo, Jianping Shi, and Xiaou Tang. Two at once: Enhancing learning and generalization capacities via ibn-net. In *Proceedings of the European Conference on Computer Vision (ECCV)*, pages 464–479, 2018. [1, 3, 6](#)

[31] Xingang Pan, Xiaohang Zhan, Jianping Shi, Xiaou Tang, and Ping Luo. Switchable whitening for deep representation learning. In *Proceedings of the IEEE/CVF International Conference on Computer Vision*, pages 1863–1871, 2019. [1](#)

[32] Duo Peng, Yinjie Lei, Munawar Hayat, Yulan Guo, and Wen Li. Semantic-aware domain generalized segmentation. In *Proceedings of the IEEE/CVF Conference on Computer Vision and Pattern Recognition*, pages 2594–2605, 2022. [1, 2, 3, 6, 7](#)

[33] Duo Peng, Yinjie Lei, Lingqiao Liu, Pingping Zhang, and Jun Liu. Global and local texture randomization for synthetic-to-real semantic segmentation. *IEEE Transactions on Image Processing*, 30:6594–6608, 2021. [1, 3, 6, 7](#)

[34] Stephan R Richter, Vibhav Vineet, Stefan Roth, and Vladlen Koltun. Playing for data: Ground truth from computer games. In *European conference on computer vision*, pages 102–118. Springer, 2016. [1, 5](#)

[35] Herbert Robbins and Sutton Monro. A stochastic approximation method. *The annals of mathematical statistics*, pages 400–407, 1951. [6](#)

[36] German Ros, Laura Sellart, Joanna Materzynska, David Vazquez, and Antonio M Lopez. The synthia dataset: A large collection of synthetic images for semantic segmentation of urban scenes. In *Proceedings of the IEEE conference on computer vision and pattern recognition*, pages 3234–3243, 2016. [1, 5](#)

[37] Gabriel Tjio, Ping Liu, Joey Tianyi Zhou, and Rick Siow Mong Goh. Adversarial semantic hallucination for domain generalized semantic segmentation. In *Proceedings of the IEEE/CVF Winter Conference on Applications of Computer Vision*, pages 318–327, 2022. [3](#)

[38] Yi-Hsuan Tsai, Wei-Chih Hung, Samuel Schulter, Ki-hyuk Sohn, Ming-Hsuan Yang, and Manmohan Chandraker. Learning to adapt structured output space for semantic segmentation. In *Proceedings of the IEEE conference on computer vision and pattern recognition*, pages 7472–7481, 2018. [2](#)

[39] Dmitry Ulyanov, Andrea Vedaldi, and Victor Lempitsky. Improved texture networks: Maximizing quality and diversity in feed-forward stylization and texture synthesis. In *Proceedings of the IEEE conference on computer vision and pattern recognition*, pages 6924–6932, 2017. [3](#)

[40] Tuan-Hung Vu, Himalaya Jain, Maxime Bucher, Matthieu Cord, and Patrick Pérez. Advent: Adversarial entropy minimization for domain adaptation in semantic segmentation. In *Proceedings of the IEEE/CVF Conference on Computer Vision and Pattern Recognition*, pages 2517–2526, 2019. [2](#)

[41] Qi Xu, Liang Yao, Zhengkai Jiang, Guannan Jiang, Wenzheng Chu, Wenhui Han, Wei Zhang, Chengjie Wang, and Ying Tai. Dirl: Domain-invariant representation learning for generalizable semantic segmentation. In *Proceedings of the AAAI Conference on Artificial Intelligence*, volume 36, pages 2884–2892, 2022. [3](#)

[42] Fisher Yu, Haofeng Chen, Xin Wang, Wenqi Xian, Yingying Chen, Fangchen Liu, Vashisht Madhavan, and Trevor Darrell. Bdd100k: A diverse driving dataset for heterogeneous multitask learning. In *Proceedings of the IEEE/CVF conference on computer vision and pattern recognition*, pages 2636–2645, 2020. [5](#)

[43] Xiangyu Yue, Yang Zhang, Sicheng Zhao, Alberto Sangiovanni-Vincentelli, Kurt Keutzer, and Boqing Gong. Domain randomization and pyramid consistency: Simulation-to-real generalization without accessing target domain data. In *Proceedings of the IEEE/CVF International Conference on Computer Vision*, pages 2100–2110, 2019. [1, 2, 3, 6](#)

[44] Jian Zhang, Lei Qi, Yinghuan Shi, and Yang Gao. Generalizable semantic segmentation via model-agnostic learning and target-specific normalization. *arXiv preprint arXiv:2003.12296*, 2(3):6, 2020. [2](#)

[45] Pan Zhang, Bo Zhang, Ting Zhang, Dong Chen, Yong Wang, and Fang Wen. Prototypical pseudo label denoising and target structure learning for domain adaptive semantic segmentation. In *Proceedings of the IEEE/CVF Conference on Computer Vision and Pattern Recognition*, pages 12414–12424, 2021. [5](#)

[46] Yuyang Zhao, Zhun Zhong, Na Zhao, Nicu Sebe, and Gim Hee Lee. Style-hallucinated dual consistency learning for domain generalized semantic segmentation. In *Computer Vision–ECCV 2022: 17th European Conference, Tel Aviv, Israel, October 23–27, 2022, Proceedings, Part XXVIII*, pages 535–552. Springer, 2022. [1, 2, 3, 6, 7](#)

[47] Jun-Yan Zhu, Taesung Park, Phillip Isola, and Alexei A Efros. Unpaired image-to-image translation using cycle-consistent adversarial networks. In *Proceedings of the IEEE international conference on computer vision*, pages 2223–2232, 2017. [2, 4](#)